Proceedings World Geothermal Congress 2020+1
Reykjavik, Iceland, April - October 2021

Advances in the Geothermal Exploration of the East Africa Rift System

Claudio Pasqua[1,2], MassimoVerdoya[2], Paolo Chiozzi[2], Egidio Armadillo[2], Daniele Rizzello[3], Taramaeli T. Mnjokava[4]

[1]*ELC-Electroconsult, Milano Italy*

[2]*DISTAV-Università di Genova, Italy*

[3]*TELLUS Sas*

[4]*TGDC Limited*

claudio.pasqua@elc-electroconsult.com

Keywords: Geothermal play types, geophysical exploration, geochemical features

ABSTRACT

We review results of geological, geochemical and geophysical investigations carried out within the frame of recent geothermal surveys in the East African Rift System (EARS). In particular, we focus on three of the most important geothermal fields namely Alalobeda (Ethiopia), Menengai (Kenya) and Ilwalilo-Kilambo (Tanzania). These fields well represent the different structural, volcanological and hydrogeological realms that may be encountered in EARS. Alalobeda and Menengai are examples of two possible geothermal play types of the Eastern Branch of EARS. The former is a fault-leakage-controlled geothermal system, located in a half-graben structure, where the heat source is likely diffuse, deep-seated magmatism, associated to the lithosphere thinning that regionally affects this area. The reservoir temperature of this water-dominated system ranges from 185 to 225 °C. The Menengai geothermal field can be classified as a convection-dominated magmatic play-type, where the heat source could be a magmatic intrusion (syenitic), located beneath the caldera. A shallow, liquid-dominated reservoir (with temperatures of 150-190 °C) and intermediate-deep reservoir, hosting steam and liquid (with temperatures of 230-340 °C) were detected. The Ilwalilo-Kilambo field is geothermal system located in a half-graben realm, in which the ascending groundwater flow is controlled by the main regional fault. Reservoir temperatures are of about 110-140 °C and the source of heat is provided by the elevated mantle.

1. INTRODUCTION

The East African Rift System (EARS) is the most extensive, currently active zone of continental rifting. It is an intracontinental divergent plate boundary at which the African plate is splitting into the Nubian and Somali plates (Fig. 1). It can be divided into an Eastern and a Western Branch. To the north, the Eastern Branch includes the Afar region, the Main Ethiopian Rift (MER) and the Kenya Rift. South of the Aswa shear zone, the Western Branch starts, and the Eastern Branch tends to be less well defined. The development of the rift system largely occurred within the Proterozoic basement, at the margins of the Archean cratons of central Africa (Chorowicz, 2005).

Within each rift segment, E-W extensional faulting dominates. Extension in other orientations (NW-SE) is occasionally seen along some of the minor rifts distributing deformation away from the main rift branches, like e.g. at the Mweru and Kariba rifts. The Western Branch is seismically active along its entire length, with further distributed deformation to the west of the main rift. Earthquakes along the Eastern Branch are less frequent than along the Western Branch (Craig et al., 2011).

Based on GPS surveys, Stamps et al (2008) reported that extension in EARS is fastest at MER (~6.5 mm yr^{-1}) and decreases southwards (~4-0.1 mm yr^{-1}) across the Eastern Branch. The extension rate increases southwards (~1.5-4 mm yr^{-1}) across the Western Branch, between the Aswa shear zone and the Rungwe volcanic province.

Receiver function studies (e.g. Last et al. 1997; Dugda et al. 2005; Cornwell et al. 2010), refraction surveys (e.g. Prodehl et al. 1994, 1997), and travel-times for P_mP-phase arrivals (Camelbeeck and Iranga 1996) show that the crustal thickness along the rift increases southwards. The Moho depth is 40-44 km beneath the Western Branch and 37-42 km beneath the Eastern Branch, whereas the crust is thinner in MER and Afar region (13-28 km).

From the late Tertiary to Recent, EARS has undergone massive magmatism that is linked with asthenospheric ascent. According to Mohr (1992), during lithospheric extension, diapiric ascent of a lherzolitic asthenospheric wedge led to the generation of basaltic melts. Partial melting may occur at all levels within the diapir, producing magmas that are tholeiitic at shallow depth, transitional at intermediate levels and alkaline at larger depth.

Abundant Cenozoic volcanism in EARS is widespread in the north, especially in the Eastern Branch, but sparse in the south (Fig. 1). Volcanic activity started in the northern part of the Eastern Branch, about 30 Ma ago with uplift, whereas in the Western Branch commenced about 12 Ma ago near the Albert Rift and about 7 Ma ago in the Tanganyka Rift (Keller et al., 1994). Most of volcanoes is located along the central axis of EARS branches. Off-axis volcanoes are explained with the opening of large tension fractures caused by reactivation of Precambrian zones of weakness (Bosworth, 1987).

In the rift axis of the Eastern Branch, numerous volcanoes of Quaternary age occur, overlying products of Miocene and Pliocene volcanism. The shield volcanoes are built largely of intermediate lavas and the associated pyroclastics, thus indicating the presence of shallow, hot bodies (magma chambers). In the Western Branch, there is paucity of volcanism along the entire length of the rift

with the main volcanic areas near Kivu Rift (Virunga volcanic province) and between Rukwa and Malawi rifts, in the Rungwe volcanic province (Ebinger et al., 1989; Omenda, 2009). The Western Branch is mostly characterized by the abundance of potassic alkaline rocks that consist of carbonatites, ultrapotassic mafic rocks and potassic mafic-felsic lavas, indicating that melting was deeper than in the Eastern Branch.

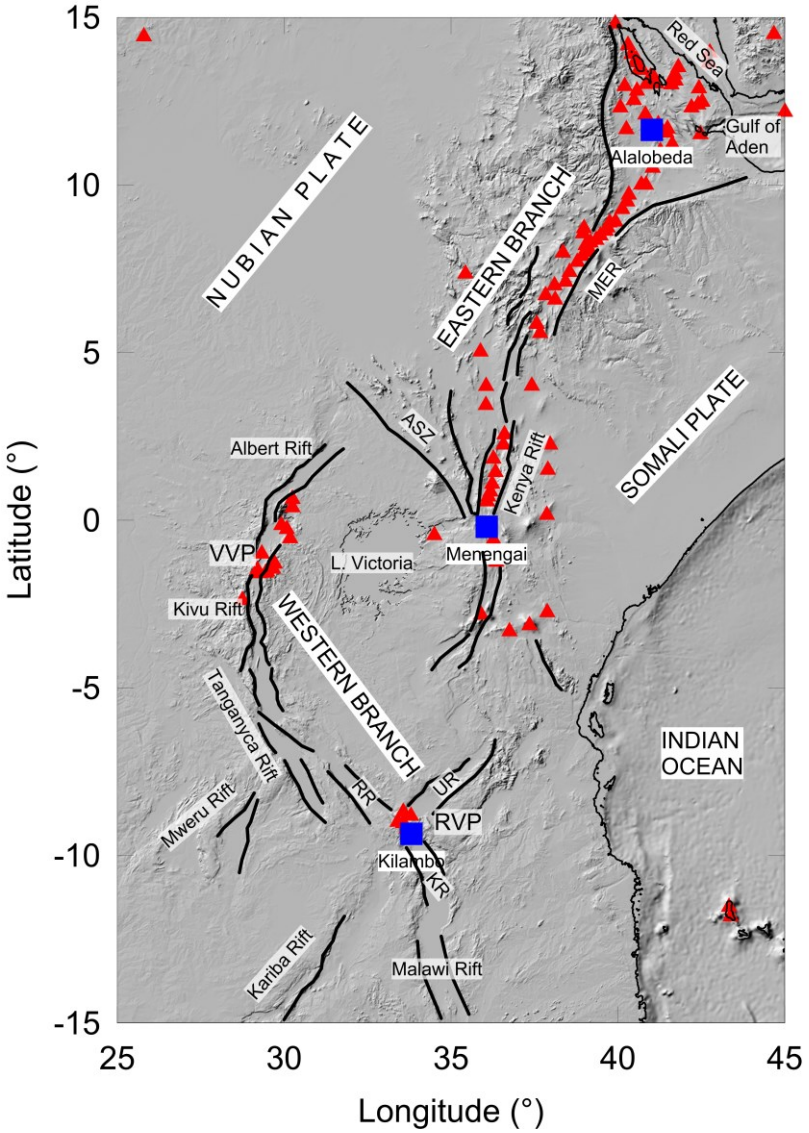

Figure 1: Structural sketch of the East African Rift System and location of the investigated geothermal fields (blue squares): MER, Main Ethiopian Rift; ASZ, Aswa shear zone; RR, Rukwa Rift; UR, Usangu Rift; KR, Karonga Rift; VVP, Virunga volcanic province; RVP, Rungwe volcanic province. Major active faults (black lines) and volcanoes (red triangles) are also shown.

These volcanological and structural features, together with the high heat flow, associated with magmatic activity and hydrothermal circulation, make EARS Africa's largest geothermal potential area. Hot springs, fumaroles, and steaming grounds are more abundant in the Eastern Branch (Afar, MER and Kenya Rift) where shallow magma bodies are the most likely heat sources for volcano-hosted high-temperature geothermal systems. In the Western Branch, off the sparse Quaternary volcanic centers, deep circulation of ground water through the rift master faults, coupled with heating by young dike intrusions or plutons, is the most likely mechanism for explaining some of the geothermal systems (Omenda, 2013).

In view of the structural and volcanological differences between the two branches of the rift system, a classification of EARS geothermal plays according to conventional schemes can be hardly applied, as the geothermal systems often exhibit hybrid characteristics (Moeck, 2014). Although all play types of EARS are convection-dominated, it is difficult to distinguish between magmatic and extensional domain play types, as extension causing thinning of the crust may coexists with formation of magmatic intrusions.

In this paper, we review geological, geochemical and geophysical results and present new data and interpretations of recent explorations of geothermal resources in EARS. In particular, we focus on three of the most important geothermal fields (Alalobeda, Menengai and Ilwalilo-Kilambo) of the Eastern and Western branches (Fig. 1). These fields well represent the different structural, volcanological and hydrogeological realms that may be encountered in EARS.

The geothermal field of Alalobeda (Ethiopia) is located on the western flanks of a rift zone, in the neighbouring of the Afar triple junction. Geoscientific exploration was recently carried out in the framework of a project of evaluation of the geothermal resources of the country (ELC-GSE, 2016). The Menengai geothermal field (Kenya) is located in a recent caldera, resulting from the intersection of minor rifts with the Kenya Rift that is sometimes considered to be the surface evidence of a mantle plume (Omenda, 2010). A series of investigations was carried out to evaluate the potential and the possible development of this geothermal field (ELC-GDC, 2015). The Ilwalilo-Kilambo geothermal area (Tanzania) is located along a NW-SE trending fault system in the Rungwe Volcanic Province (RVP). In view of the national interest in the use and development of geothermal energy, a project was started aimed at increasing the knowledge of this geothermal field (ELC-TGDC, 2017).

The data collected within the several surveys allow us to propose conceptual models of each field that give an insight into of the variability of geothermal plays occurring in the different parts of EARS. This can be of help in planning future studies and define optimal procedures of geothermal resource exploration in EARS.

2. ALALOBEDA

The Alalobeda geothermal field is located in the western sector of the Tendaho Graben (Fig. 2). Pliocene-Pleistocene basaltic rocks, belonging to the Afar Stratoid Series (ASS) are the main lithotype. ASS basalts have an estimated thickness of 1500 m (Abbate et al., 1995; Acoccella et al., 2008) and are covered by young sedimentary deposits (fluvio-lacustrine sediments of the Tendaho Graben), with local intercalations of basaltic levels. Beneath ASS, the Dahla Formation (DF), composed of an association of basalt with intercalation of ignimbrite and sediment, occurs. DF does not crop out in the Alalobeda area, but it was encountered in drilled shallow and deep wells in the Dubti-Ayrobera geothermal area, 20 km NW of Alalobeda (Battistelli et al., 2002). This structural pattern is well visible in the ASS outcrops and is dominated by a NW-SE main system of faults following the Red Sea system, and the NNE-SSW faults system related to the tectonics of MER.

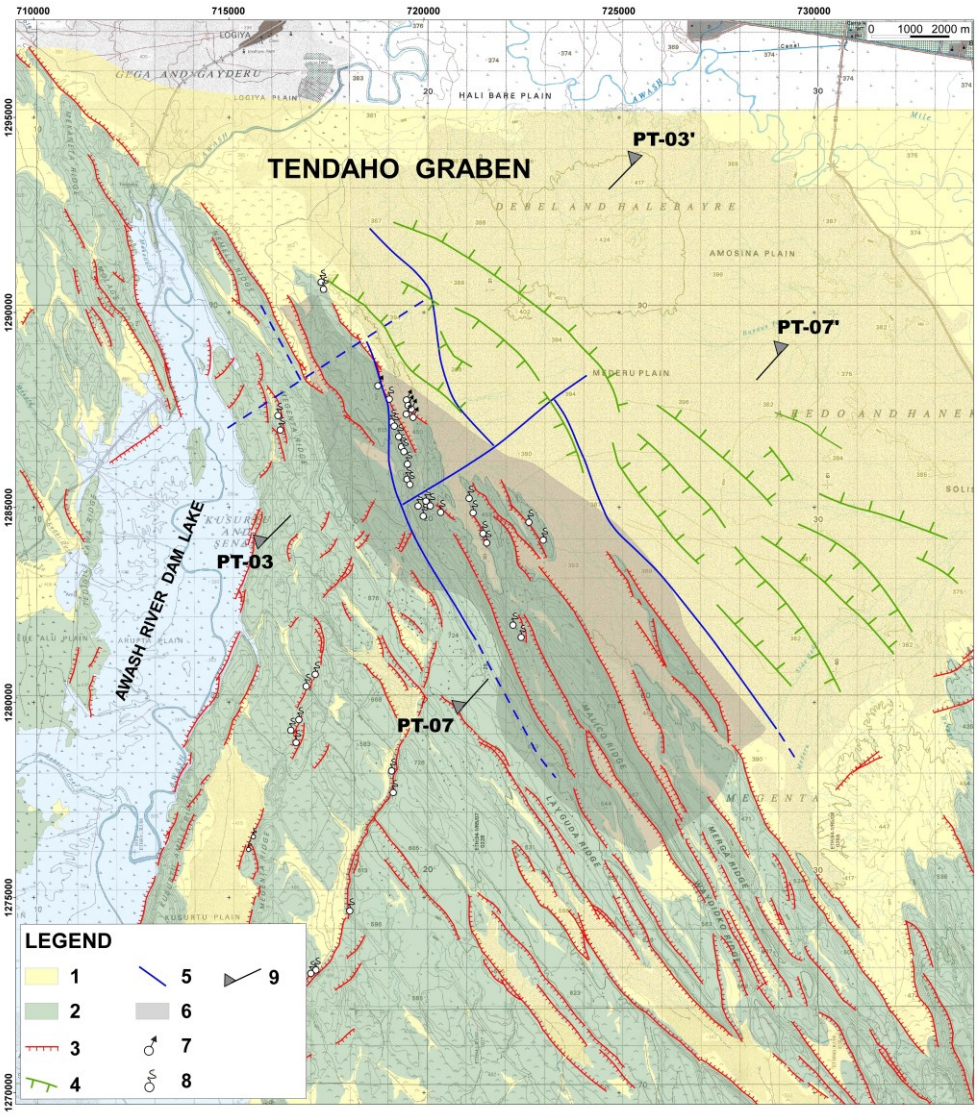

Figure 2: Geological map of the Alalobeda geothermal field. Young sedimentary deposits (1); basaltic rocks of the Afar Stratoid Series (2); main faults inferred from the geological survey (3); faults inferred from the gravity survey (4); faults inferred from the magnetotelluric survey (5); positive Bouguer anomaly (6); hot spring (7); fumarole/steaming ground (8); cross-sections (9).

2.1 Geophysical and geochemical data

In the Alalobeda field, the picture of the fracture systems inferred from geological observations was recently integrated by results of three-dimensional magnetotelluric (MT) and gravity data inversion (Rizzello et al., 2016). In particular geophysical results showed that the NW-SE normal fault system also continues beneath the sediments and it is offset by NE-SW trending transversal lineaments that may be interpreted as strike-slip faults. Beneath the Tendaho Graben shoulder, a positive density contrast that may correspond to propylitic alteration of ASS was modelled at depths between 1 and 2 km.

The resistivity model showed that the NNE-SSW trending fracture zones, beneath the shoulder of the graben, continues at depth, but they appear interrupted by the NW-SE main normal fault system. The 3D resistivity model also revealed a deep conductivity anomaly extending to about 4000 m depth in the central part of the investigated area.

Microseismicity data (Pasqua, 2019) show that earthquakes are rather frequent, mostly shallow and of low magnitude (<4.0). The maximum density of earthquakes was recorded in a NW-SE elongated zone, well matching the maximum concentration of hot springs. Below 5 km depth, a clear seismic cut-off was observed. This can be interpreted as the brittle-ductile transition that, for a continental crust, should correspond to 350-600 °C (Maggi et al., 2000; Pasquale et al., 2010). Seismicity above this zone may be related to the hydrothermal circulation, which may activate the existent fractures.

Hot springs, mostly clustered within a narrow zone (700 x 350 m), and fumaroles tend to concentrate along or at the intersection of NNE-SSW and NNW-SSE trending faults (Fig. 2). Sodium-chloride type, similar to those found in the exploratory wells of the nearby Dubti-Ayrobera geothermal field (Didana et al., 2015), and sodium-bicarbonate type waters were sampled at the hot springs. Based on the *Na-K* and *K-Mg* geothermometers (Giggenbach, 1988), all samples indicate that the reservoir is close to equilibrium with albite, K-feldspar, chlorite, illite and silica at 200-220 °C. Such temperature is substantially consistent with that inferred from fumaroles gases (on average 185-225 °C). Both the estimated temperatures and the isotopic composition, which exhibits a relatively low oxygen isotope shift, suggested a water-dominated reservoir. The isotopic composition of the geothermal fluids, compared with the isotopic values of the Ethiopian rainwater, suggested that the reservoir hosts paleowater (Pasqua et al., 2016).

The lack of manifestations in the graben plain does not necessarily mean that ground water flow does not occur in this zone. This could be partly due to the impervious surface sediment, which may hinder the upwelling of geothermal fluids. However, the sedimentary sequence alone is too thin (~100-200 m) to impede the escape of the geothermal fluids. Thus, the ASS basalts, together with sediments, may play the role of cap-rock while the underlying DF would act as reservoir. ASS basalts exhibit very low resistivity values (<5-10 Ω m), but surprisingly there is no evidence of alteration. The low resistivity could be explained in terms of interaction between magma and sediments, which may result in a mixed material referred to as peperite (e.g. Waichel et al., 2007).

2.2 Integrated interpretative model

From the interpretation of the available data, we argue that the geothermal reservoir is likely located below the major hot springs and enclosed between the fractures trending NNW-SSE and the geoelectrical discontinuities trending WSW-ENE (Fig. 2). Within this zone, the seismic events are more frequent and the focal depths are shallower.

Figure 3 presents two cross sections (PT03 and PT07) that summarize the geoscientific data reported by Rizzello et al. (2016) and the likely conceptual model of the Alalobeda field. The area overlying the reservoir (cross-section PT-03) shows an upper unit w)th low electrical resistivity of 1-10 Ω m and average thickness of 1000 m, that may be interpreted as the cap-rock of the geothermal system. Below this unit, resistivity increases to values of ~100 Ω m. This value is higher than the values of 20-50 Ω m normally characterizing geothermal reservoirs (e.g. Pellerin et al, 1996; Ussher et al., 2000; Anderson et al., 2000). In the central part of the investigation area (cross-section PT-07), a wide low-resistivity zone (< 30 Ω m) extends to large depth and might be interpreted as an alteration zone caused by upward flow. We suggest that geothermal fluids might migrate from the upward flow zone towards the reservoir driven by the NNW-SSE fault system. The fracture system might also act as an impervious barrier preventing fluid flow in WSW and ENE directions.

The fluid chemical composition suggests that the Alalobeda geothermal system has no connection with the nearby Dubti system. Geological and geophysical observations did not argue for a shallow geothermal aquifer (similar to that of Dubti). This is likely due to the impervious nature of the shallow layers.

In the Dubti-Ayrobera areas, Stimac et al. (2014) and Didana et al. (2015) claimed that a large intrusive magmatic body, fed by deep mantle sources, is the heat source of the geothermal system. This conclusion was based on results of MT inversions that identified a low-resistivity 15-km-wide body at a depth of 5-18 km. MT data from Alalobeda, albeit of good quality, could not resolve the resistivity structure at depths larger than 5 km (Rizzello et al., 2016). Thus, the occurrence of such a deep and huge conductor can be neither proved nor disproved. However, we noticed that the seismic cut-off depth is nearly uniform across the area. Consequently, we may argue that a single magmatic body intrusion in the shallow crust is unlikely. We suggest that diffuse, deep-seated magmatism, related to the lithosphere thinning that regionally affects this area (e.g.Tessema and Antoine, 2004) could be rather the heat source in the Alalobeda as well as in the Dubti-Ayrobera geothermal systems.

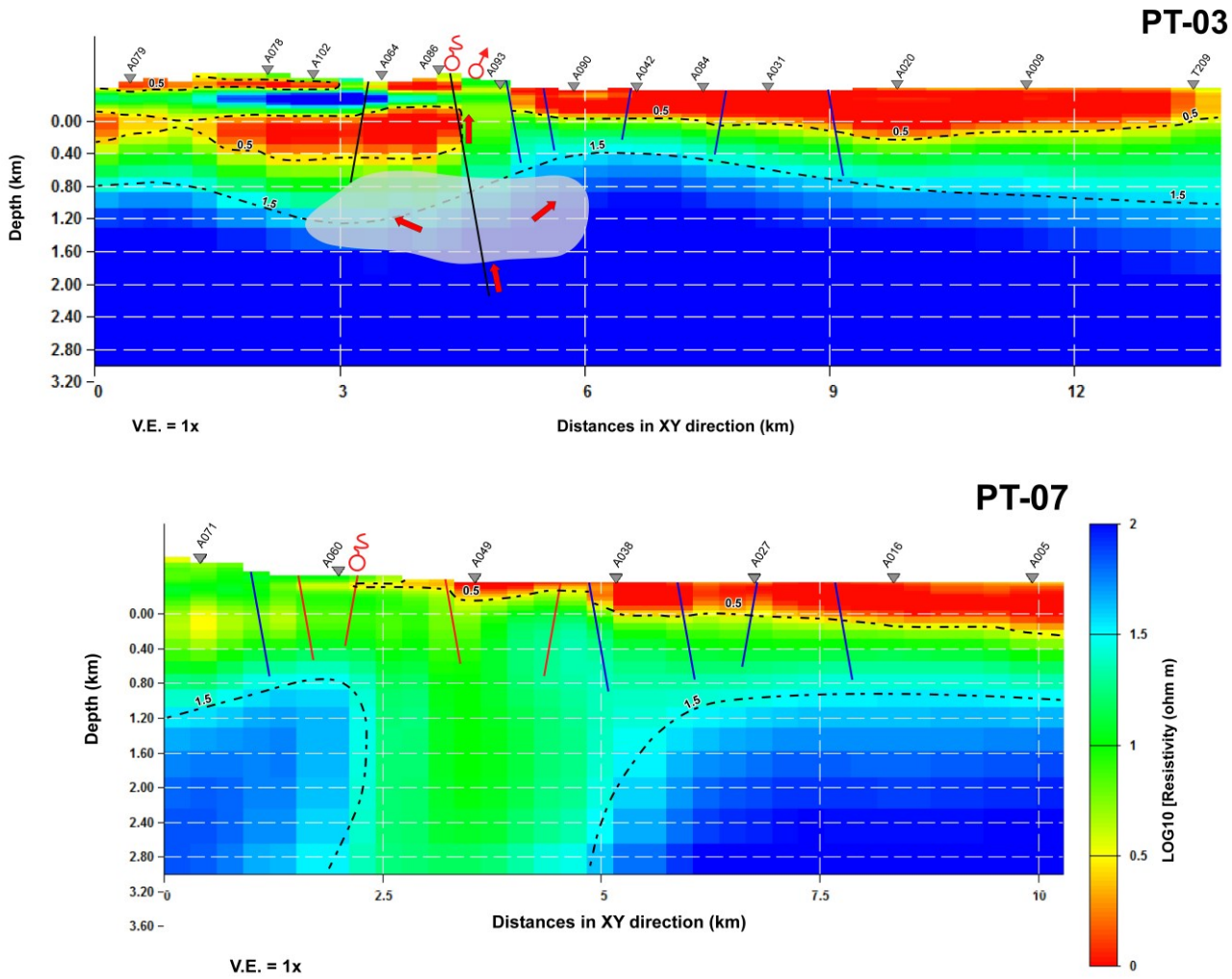

Figure 3: Conceptual model of the Alalobeda geothermal field along the resistivity cross-sections PT03 and PT07. The location of the tectonic lineaments inferred from the geological study (red lines), MT (blue lines) and gravity surveys (green lines) are indicated. The shaded area is the geothermal reservoir. Black triangles are the MT stations. Red arrows, ground water upflow. Fumaroles and hot springs are also indicated (see Fig. 2 for symbols)

3. MENENGAI

The geological and structural pattern of the Menengai caldera, laying in the central part of the Kenya Rift, is presented in Fig. 4. Volcanism has been active since 29 ka ago as testified by a huge ash flow deposited in the surrounding lakes (Leat, 1984; Mungania, 1999). After this event, the volcanic edifice evolved into the present-day caldera. The formation of the caldera top and of a huge amount of trachytes is related to another important eruption that dates back to 8 ka ago. From the numerous ash flows occurring within the caldera, Mibei and Lagat (2011) inferred that last eruption took place a few hundred years ago.

The lithotypes cropping out within the caldera and those intersected by the several wells that were drilled in the last decade are blocky lavas of peralkaline-trachytic composition with subordinate pyroclastic intercalations (Omondi, 2011; ELC-GDC, 2013). Intrusive products progressively increase with depth and towards the central portion of the caldera (Lagat, 2011). Erratic lenses of syenitic intrusive and basaltic rocks were also encountered in some wells, suggesting that magma pulses were injected into the overlying formations in the form of dikes (GDC, 2018).

The area is affected by a complex pattern of tectonic lineaments, likely resulting from intense neo-tectonic activity. The dominating fault system, resulting from a remote sensing analysis (ELC-GDC, 2013; Kanda et al., 2019), trends NNW-SSE and is well aligned with eruption centers and fumaroles activity. Another important system has roughly E-W direction. Several additional secondary fracture systems with different orientations were also inferred from remote sensing analysis and field observations. Fumaroles, steaming grounds and the hot fluids found in the boreholes are evidence of hydrothermal activity and of occurrence of a geothermal reservoir.

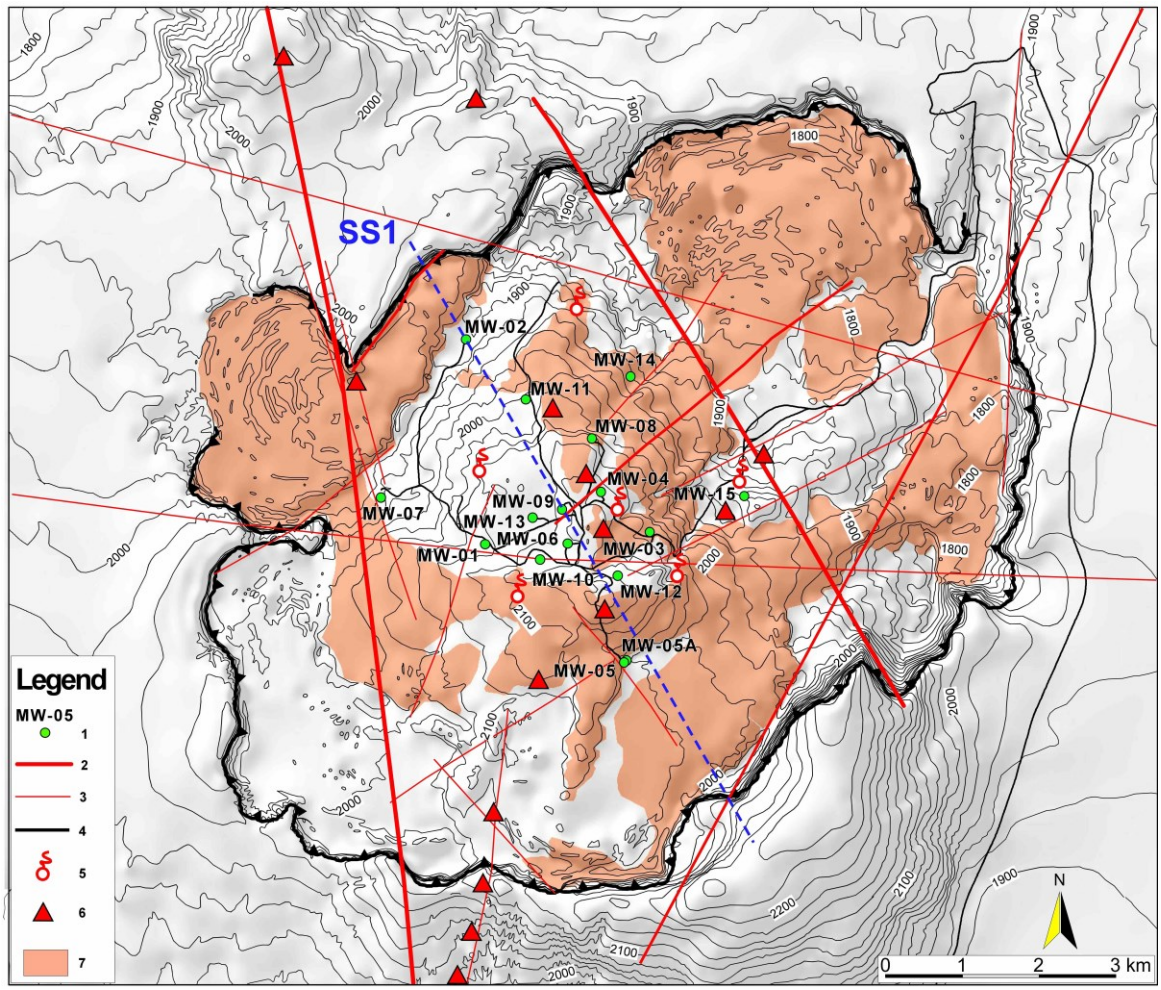

Figure 4: Geological sketch of the Menengai caldera. 1, boreholes; 2, major fault; 3, lineament and fault; 4, caldera rim; 5, fumarole; 6, eruption centre; 7, blocky lava. The trace of the section SS1 is showed.

3.1 Geophysical and geochemical data

Gravity and MT data were available within the Menengai caldera an its surroundings (Wamalwa et al., 2013; ELC-GDC, 2013; Montegrossi et al., 2015). The analysis of gravity data puts into evidence a well-pronounced positive anomaly in correspondence of the Menengai caldera. The anomaly can be modeled with a higher density body (2900 kg m^{-3}) below the caldera (Fig. 5). The density of the body is compatible with gabbroic composition, perhaps formed from cumulates associated with differentiation of a mafic (basaltic) magma. This picture is consistent with seismic travel-time data (Henry et al. 1990) and the seismic and gravity models by Simiyu and Keller (2001), indicating a high-velocity basement.

2-D inversion of MT data revealed three stratigraphic units: (i) an uppermost resistive unit (50-100 Ω m), with a thickness of 100-300 m; (ii) an underlying upper conductive unit (< 5 Ω m), with an average thickness of 600-800 m (iii) a "resistive basement" (> 30 Ω m). The high-density magmatic body at depth was not revealed by MT modelling. Since resistivity decreases with temperature, this argues that the magmatic body might be still hot. Additional evidence of anomalous temperature at depth, was given by micro-seismicity monitoring of the zone centered on the Menengai caldera (Simiyu, 2009), that showed that the maximum depth of earthquakes is about 3500-4000 m. This depth corresponds well to the top of the high-density body inferred from gravity (Fig. 5).

All thermal water samples from wells and hot springs belong to the *Na-HCO_3* facies. Geochemical analysis of these samples and of soil gases (ELC-GDC, 2013) indicated the occurrence of a shallow, liquid-dominated reservoir (with temperatures of 150-190 °C) and intermediate-deep reservoirs, at least partly hydraulically connected (with temperatures of 230-340 °C), hosting fluids at different vapor/(vapor+liquid) mass ratios. The analysis of the gas equilibrium suggests that there is an increase in vapor/(vapor + liquid) mass ratio not only horizontally, i.e. towards the caldera central zone wherein the vapor-discharging wells MW-06, MW-09, and MW-13 are located, but also with depth.

3.2 Integrated interpretative model

The availability of direct information from logging and testing of geothermal wells (see Pasqua, 2019 and references therein) was fundamental to validate the inferences of the geophysical and geochemical investigations. Figure 5 shows the conceptual model of the Menengai geothermal field obtained by integrating surface geological and geophysical information and the results of drilling.

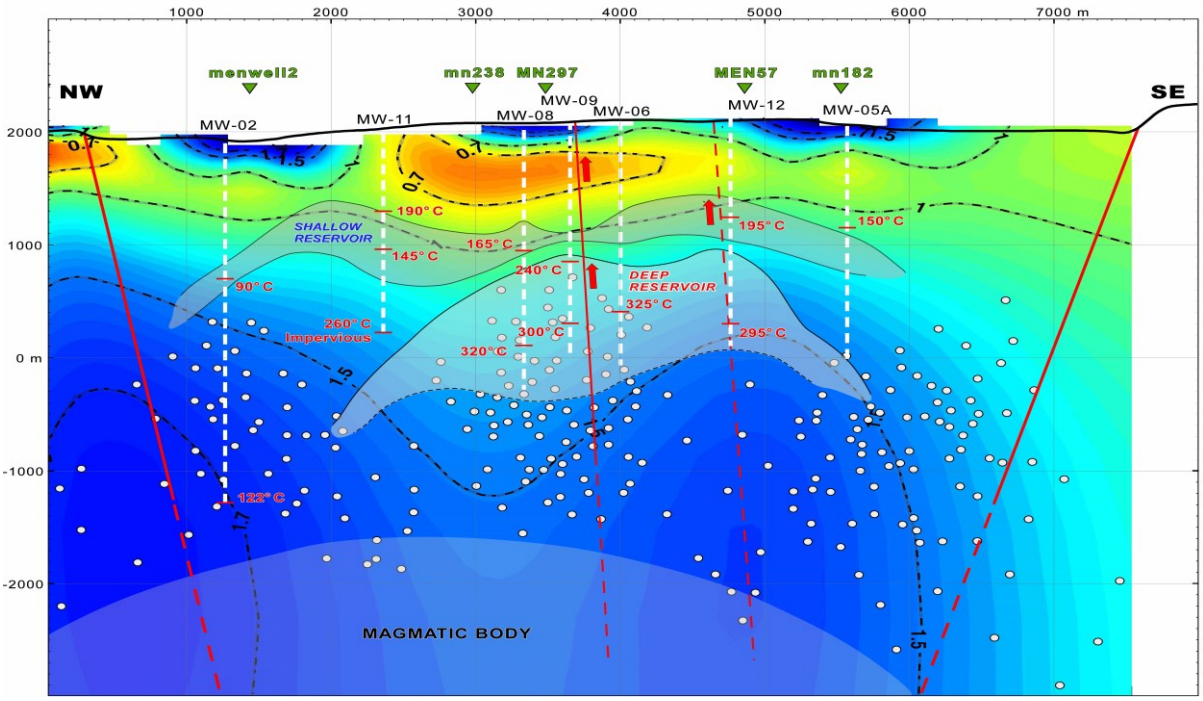

Figure 5: Conceptual model of the Menengai geothermal field along the cross-section SS1 (Fig. 4). White full circles are the earthquake foci (Simiyu, 2009). White hatched lines are boreholes (see Fig. 4 for locations); values of the measured temperatures are indicated. The red arrow is the upward flow along the main faults (red line). Green triangles are the MT stations. Dashed black line are isoresistivity contour line in Log10 resistivity (Ohm m).

The stratigraphic sequence, inferred from the boreholes, consists predominantly of trachytic lava. Thus, the degree of hydrothermal alteration and tectonic fracturing controls the permeability. The low-resistivity (<10 Ω m) layer at shallow depth (600-1000 b.g.l.) may represent the cap-rock of the reservoir. This layer is rather discontinuous and hosts a shallow and relatively cold aquifer. The geothermal reservoirs found by boreholes are hosted within the 1500-2000 m thick zone with resistivity 10-30 Ω m. These values are somehow slightly lower that those typical of a reservoir.

Borehole logs confirm the occurrence of two distinct reservoirs: (i) a shallow, liquid-dominated reservoir of reduced thickness, sometimes encountered by the wells (in particular MW-06 and MW-09); (ii) a deeper vapor-dominated reservoir, crossed by boreholes MW-06, 08, 09, and 12. The vapor phase tends to reduce laterally, in good agreement with the geochemical data. Boreholes MW-02 and MW-05A, generally showing lower temperatures (90-150 °C) indicate that both the shallow and deep reservoir thin laterally.

Measurements of performance in the Menengai wells showed extremely high temperatures, often above 300°C and reaching supercritical values up to 390°C at the hole bottom, and presence of multiple feed zones over extended wellbore sections. The boreholes temperatures are generally in good agreement with the temperatures inferred from the geochemical data, even if some apparent deviations occur. In borehole MW-02, a temperature of only 90 °C was recorded in the shallow reservoir, and at the bottom hole (about 3000 m depth b.g.l.) the temperature was only about 120 °C. The temperature gradient is thus very low (15 mK m^{-1}) and may indicate cooling due to leakage of cold water from the shallow aquifer.

The temperature profile of borehole MW-11 exhibited a clear inversion, i.e. a decrease from 190 °C at the top (700 m bg.l.) to 145 °C in the intermediate-lower portion (1000-1300 m b.g.l.) of the shallow reservoir. Such an inversion may be explained with lateral inflows of colder water within the reservoir. Below the reservoir bottom, the temperature linearly increases to a value of 260 °C with a gradient of about 180 mK m^{-1}, which likely characterizes the conductive (impermeable) portion of the borehole. Borehole MW-06, 08, 09 and 12 showed that the deep reservoir is characterized by temperatures ranging from 240 to 320 °C and a maximum thickness of about 1000 m can be estimated.

Permeability of both shallow and deep reservoir is strongly controlled by the fault systems that affect the caldera. This clearly turns out from the temperature recorded in boreholes MW-03. In this hole, which is located off the secondary fracture system (Fig. 4), temperatures are lower than about 35-100 °C with respect to the other boreholes and the temperature gradient is similar to that of borehole MW-02, and permeability is limited to very thin levels.

The integrated analysis of micro-earthquake distribution and gravity indicates that the heat source of the geothermal system may be located at 3500-4000 m depth, corresponding to the high-density body inferred from gravity modelling. The seismic cut-off occurring at this depth roughly tracks the upper boundary of the high-density body. If we assume a temperature gradient of 180 mK m^{-1}, i.e. that characterizing the impervious zone beneath the deep reservoir, the expected temperature at the top of the high density body should be about 650 °C. This inferred temperature well matches the expected limit of the brittle-ductile transition (Maggi et al., 2000; Pasquale et al., 2010) and is in agreement with the conclusion by Simiyu (2009) that partially molten material may occur at depths between 5 and 6 km. Seismicity above the brittle-ductile transition seems associated to the main fault systems.

Due to a lack of isotopic data of fluids from the deep wells, no information was available on the nature of the deep reservoir recharge water. It is likely that the recharge takes place along the borders of the caldera, in correspondence of the major tectonic structures, which may favor the deep infiltration of meteoric water, with minor contribution from the magmatic system in the form of steam and gas transfer. The main zone of upward flow is situated in the central part of the caldera, and the two major faults running NNW-SSE might act as a hydrogeological barrier.

4. KILAMBO-ILWALILO

The Kilambo-Ilwalilo geothermal area (Tanzania) is located close to the eastern margin of the Karonga Rift, and it is part of the Rungwe volcanic province of the Western Branch of EARS (Fig. 1). The beginning of Karonga rifting is dated Late Miocene–Pliocene, and its volcanism and faulting propagated from south to north since 7 Ma ago to present (Ebinger et al., 1993).

The main geothermal manifestations are the hot springs located along the Mbaka fault (Fig. 6), namely Kilambo, Kajala and Ilwalilo (Mnjokava et al., 2018). The hot springs of Kilambo and Kajala exhibit a total flow rate of 0.015 $m^3 s^{-1}$, with temperatures of 59-64 °C , producing a thermal discharge of 2.5 MW. The hot springs at Ilwalilo has outlet temperature up to 64 °C, flow rate of at least 0.005 $m^3 s^{-1}$ and 0.8 MW of thermal yield. The Lufundo and Kiejo gas vents are other evidence of geothermal activity.

The oldest formation cropping out in the area consists of a metamorphic basement, including ortho-gneisses, meta-anorthositic and amphibolitic rocks. This unit occurs in the NE side of the Mbaka Fault (Fig. 6), and presents a pronounced schistosity and a fine network of fractures. Consequently, its secondary permeability can be fair. South-west of the Mbaka fault, the basement is covered by Mesozoic sediment. This unit does not crop out in the investigated geothermal area. East of the Mbaka fault, Neogene-Recent volcanics (trachitic-phonolitic ignimbrites, basaltic lavas and basalts) only a few hundred metre thick, and sedimentary (siltstones and sandstones) occur, overlain by lacustrine deposits (Ebinger et al., 1989 and 1993). Several volcanic centres are present in the area and the tectonic setting is dominated by the NNW-SSE trending Mbaka fault, with secondary N-S and NE-SW trends.

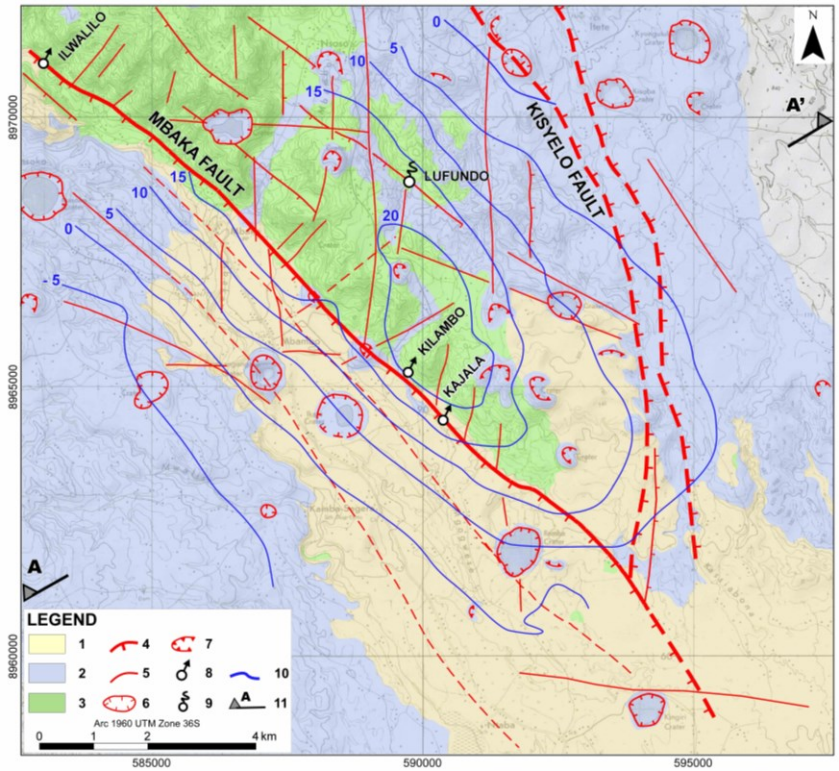

Figure 6: Geological map of the Kilambo-Ilwalilo geothermal field. 1) sediment cover; 2) volcanics; 3) metamorphic basement ; 4) major fault (dashed when inferred from geophysical data) with indication of downthrown side; 5) minor fault (dashed when inferred) with no clear indication of downthrown side; 6, Maar crater rim; 7, Cinder cone crater rim; 8, hot spring; 9, fumarole; 10) contour kines of the residual Bouguer anomaly (in mGal); 11; Cross-section.

4.1 Geophysical and geochemical data

So far, in the Karonga Basin area only data from a regional gravimetric survey were available (Ebinger et al., 1993). MT and gravity surveys were recently carried out in the Kilambo-Ilwalilo geothermal area (ELC-TGDC, 2017; Rizzello et al., 2018). Magnetotelluric measurements were carried out at 76 stations, located along 8 profiles, with a station spacing of 750 m. A more detailed sampling was set around the Kilambo thermal springs. The gravity survey, consisting of 108 stations, was performed, with a nominal spacing of 700 m along 9 lines. To evaluate the regional gravity field, twenty-five additional stations were acquired up to at a distance of about 30 km around the prospect. The dense station grid allowed for a detailed geophysical 2D and 3D modelling.

The results of MT 3D inversion showed a resistive body (100-1000 Ω m) in the central portion of the survey area that extends from ground level to depth > 4 km and can be identified as the metamorphic basement cropping-out. The high-resistivity body is surrounded by two conductive zones (<10 Ω m). In the western part of the survey area, the conductive layer is continuous and of

larger thickness (~1000 m), whereas in the eastern part it is thinner and discontinuous. Above the conductive zones, the observed resistivity of about 50-100 Ω m in the uppermost hundred meters is ascribable to the Neogene volcanic products cropping out. Towards the SE corner of the investigated area, the conductive zone becomes continuous and homogeneously thick, well matching the presence of lacustrine sediments.

Processing of gravity measurements produced a regional field similar to those reported by Ebinger et al. (1993), denoting a wide, NW-SE trending, Bouguer anomaly minimum of -160 mGal. The residual Bouguer anomaly shows positive values (>15 mGal) in the central part of the survey area, where the hot springs occur (Fig. 6). The positive anomaly can be associated to the high-density, high-resistivity metamorphic basement. East and west of the gravity high, the residual Bouguer anomaly becomes slightly negative, with a minimum value of -5 mGal.

Data on the geochemical features of the Kilambo-Kajala and Ilwalilo hot springs are reported by ELC-TGDC (2018) and Pasqua (2019). The Kilambo-Kajala reservoir has *Na-HCO₃* chemical composition, likely due to the interaction of meteoric waters with the basement rocks, sustained by conversion of CO_2 to HCO_3. The silica geothermometer indicates a reservoir temperature of about 140 °C. $\delta^{13}C$ values of CO_2 range from -5.5 to -6.0 ‰, suggested that CO_2 is chiefly supplied by deep sources (Pasqua, 2019). Ilwalilo has the same *Na-HCO₃* chemical composition and, consequently, groundwater likely circulates in rocks of the same type as in Kilambo-Kajala. The reservoir temperature is about 110 °C, as indicated by both silica and *K-Mg* geothermometers. $\delta^{13}C$ values of CO_2 (-5.6 to -6.4 ‰) point to a deep origin. The type of thermal manifestations, their chemical and isotopic characteristics and estimated temperatures suggest a water-dominated geothermal system.

Besides water sampling, soil gas monitoring was also carried out by ELC-TGDC (2018) at the hot spring sites and at Lufundo (see Fig. 6 for location). The total output of deep CO_2 was estimated of 12.7 tons/day for Kilambo-Kajala, 0.22 tons/day for Ilwalilo, 43.0 tons/day for Lufundo. The spatial distribution of the CO_2 flux was in good agreement with the NW-SE trending faults/fractures of the Mbaka system and the N-S oriented tectonic structures. Moreover, the hot springs are characterized relatively low CO_2 fluxes. On the contrary, in Lufundo, where hot springs are absent, CO_2 flux was higher, with a maximum value of 221 $mol \cdot m^{-2} \cdot day^{-1}$.

4.2 Integrated interpretative model

A cross-section summarizing all the information obtained from the geological, geophysical and geochemical investigations is presented in Fig. 7. The main feature is the low resistivity layer (< 5 Ω m), SW of the Mbaka fault, laying beneath a superficial, medium-resistivity layer, corresponding to Neogene-Recent volcanics. The low resistivity layer might be interpreted as an alteration zone (clay cap) possibly caused by hydrothermal activity affecting the Mesozoic sediment occurring beneath the Neogene-Recent volcanics and at least the shallow part of the underlying metamorphic basement.

Beneath the conductive zone, a reservoir is not clearly visible from MT modeling, as resistivity increases regularly with depth. It might lie between the 5 and 50 Ω m isoresistivity lines, at about -1000 m a.s.l., and consequently may be rather thin (~ 500 m). The Mbaka fault may act as a permeability barrier and thus define the eastern boundary of the reservoir. The other boundaries are difficult to locate and, at the present stage of investigation, any hypothesis is speculative.

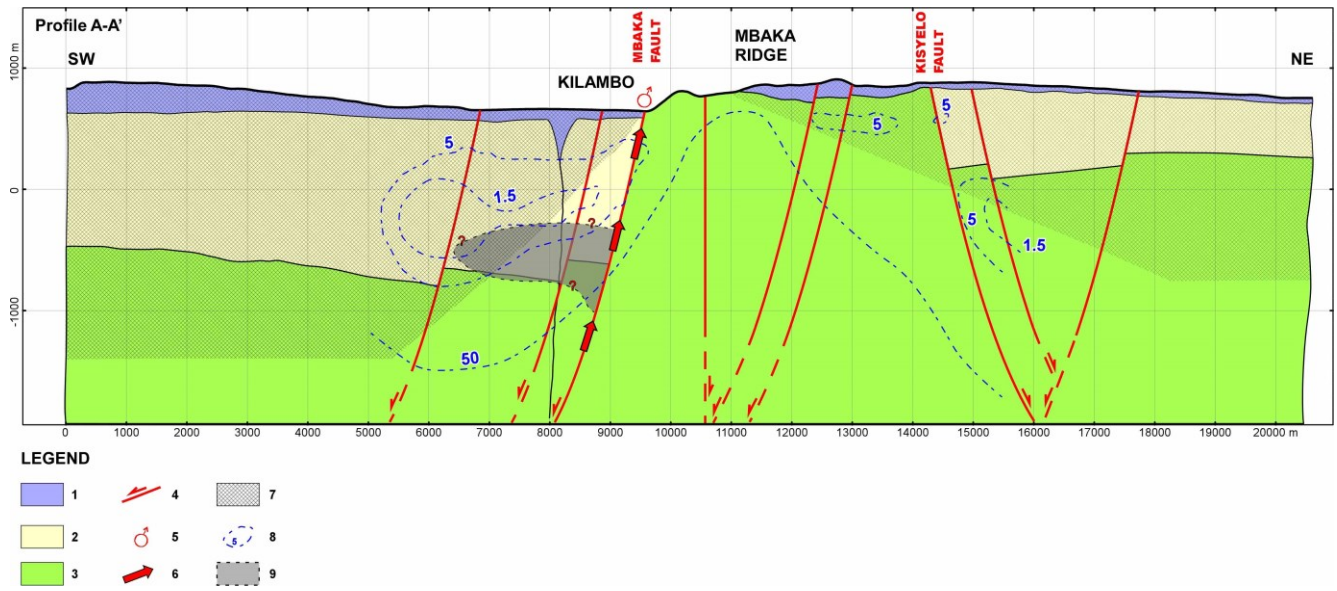

Figure 7: Geological cross-section and conceptual model of the Kilambo-Ilwalilo geothermal field. 1, Neogene-Recent volcanics; 2, sedimentary cover; 3, metamorphic basement; 4, main fault; 5, hot spring; 6; upward flow; 7, low-density layers as inferred from gravity modelling; 8, resistivity (in Ω m); 9, geothermal reservoir.

Resistivity increases abruptly (one-two orders of magnitude) east of the Mbaka fault, thus indicating that the metamorphic basement is characterized by no alteration. At the NE end of the cross-section, where Lufundo gas vents are located, a thin and discontinuous low-resistivity zone, matching the outcrops of volcanic materials, appears over the high resistivity basement. This is evidence that the gas vents do not belong to the same hydrothermal manifestations (hot springs) which are controlled by the Mbaka fault. The occurrence of another probable fault system (Kisyelo) may be supposed from the resistivity distribution.

Forward 2-D gravity modelling (Rizzello et al. 2018) indicates that the gravity high can be accounted for by a positive density contrast of 500 kg m^{-3}, corresponding to the metamorphic basement rocks. Because of their small thickness, the Neogene-Recent volcanic rocks alone cannot explain the gravimetric lows at both sides of the cross-section (Fig. 7). Therefore, the lower density layer should be as thick as about 1.5-2.0 km and might affect the Mesozoic sediments and part of the metamorphic basement. It could be interpreted as a low-temperature alteration zone and/or groundwater circulation in the Mesozoic sediment and partly in the metamorphic basement. In general, there is a good agreement between the inferred resistivity and density structure, putting into evidence the extension at depth of the Mbaka fault.

From the analysis of the regional Bouguer anomaly (Rizzello et al., 2018), there is no evidence of a magmatic heat source at least in the uppermost ~10 km depth. It is likely that the recent volcanic activity of the geothermal area and surroundings derives from very deep magma chambers. The regional negative gravity anomaly of 100-200 mGal argues for the principal source of heat related to regional lithosphere thinning. A contribution due to underplating (Ebinger et al., 1989) may also be possible, that could be supported by the high CO_2 flux of deep origin occurring in the area. The available heat flow measurements for the Karonga rift, southwest of the Kilambo-Ilwalilo area, indicate values of only about 30 mW m^{-2} (Ebinger et al., 1987), which for a thermal conductivity of about 0.7 W m^{-1} K^{-1} (Von Herzen and Vacquier, 1967) yields a geothermal gradient of 40 mK m^{-1}. Under these thermal conditions, the reservoir temperature of 110-140 °C could be reached at depth of about 3 km.

The recharge of the system is supplied by meteoric water, a likely recharge zone might be located W of the geothermal area at a distance of ~30 km. Groundwater may leak from NW to SE, warm up and flow upwards when encountering the Mbaka fault. The latter might represent the connection between the deep groundwater and the surface. West of the fault, lateral flow at intermediate depth (~1.5 km) is supported by low resistivity values (Fig. 7).

5. CONCLUSIONS

The East African Rift System (EARS) shows up as a series of thousand-kilometre-long aligned successions of adjacent individual extensional basins, characterized by recent magmatic activity and hydrothermal circulation that make EARS the Africa's largest geothermal potential area. The several branches of EARS are characterized by lateral variation of lithosphere thickness and volcanological features that are reflected by the associated geothermal fields. Among the different geothermal fields of EARS, three of them were studied in detail. They represent the different structural, volcanological and hydrogeological realms that may be encountered in EARS.

Alalobeda and Menengai fields are examples of two possible geothermal play types of the Eastern Branch of EARS. The former is a fault-leakage-controlled geothermal system, located in a graben structure, wherein the heat source is related to the occurrence of three superimposed rift systems (Red Sea, Main Ethiopian Rift and Gulf of Aden). The heat source is likely diffuse, deep-seated magmatism, associated to the lithosphere thinning that regionally affects this area. The reservoir temperature of this water-dominated system ranges from 185 to 225 °C.

The Menengai geothermal field lies in a wide caldera. It can be classified as a convection-dominated magmatic play-type. The several available thermal data recorded in boreholes together with geophysical interpretations indicate that the heat source could be a high-density magmatic intrusion with temperature of 650 °C, located at of 5-6 km depths beneath the caldera. Two reservoirs were detected: a shallow liquid-dominated reservoir, with temperatures of 150-190 °C, and intermediate-deep reservoir, hosting steam and liquid with temperatures of 230-340 °C.

A typical example of geothermal field of the Western Branch is the fault-leakage controlled geothermal system of Kilambo-Ilwalilo, located in a half-graben structure, in which groundwater flows within permeable layers, reaches the main fault and flows up and laterally. Reservoir temperatures are 110-140 °C and the source of heat is provided by mantle uplift. Despite the occurrence of eruption centres around the geothermal field, the main source of heat may be thus related to regional lithosphere thinning with a possible contribution of magmatism due to underplating.

REFERENCES

Anderson, E., Crosby, D., and Ussher, G.: Bull's eye! - Simple resistivity imaging to reliably locate the geothermal reservoir: Proceedings of the World Geothermal Congress, (2000) 909–914.

Abbate, E., Passerini, P., and Zan, L.: Strike-slip Faults in a Rift Area: a Transect in the Afar Triangle, East Africa, Tectonophysics, **241**, (1995), 67-97.

Acocella, V., Abebe, B., Korme, T., and Barberi, F.: Structure of Tendaho Graben and Manda Hararo Rift: Implications for the Evolution of the Southern Red Sea Propagator in Central Afar, Tectonics, **27**, (2008), TC4016, doi:10.1029/2007TC002236.

Battistelli, A., Yiheyis, A., Calore, C., Ferragina, C., and Abatneh, W.: Reservoir engineering assessment of Dubti geothermal field, Northern Tendaho Rift, Ethiopia, Geothermics, **31**, (2002), 381-406.

Bosworth, W.: Off-axis volcanism in the Gregory rift, east Africa: implications for models of continental rifting, Geology, **15**, (1987), 397-400.

Camelbeeck, T., and Iranga, M.D.: Deep crustal earthquakes and active faults along the Rukwa trough, eastern Africa, Geophys. J. Int., **124**, (1996), 612-630.

Chorowicz, J.: The East African rift system, J. Afr. Earth Sci., **43**, (2005), 379-410.

Cornwell, D.G., Maguire, P.K.H., England, R.W., and Stuart, G.W.: Imaging detailed crustal structure and magmatic intrusion across the Ethiopian Rift using a dense linear broadband array, Geochem. Geophys. Geosyst., **11**, (2010), doi:10.1029/2009GC002637.

Craig, T.J.. Jackson, J.A., Priestley K., and McKenzie D.: Earthquake distribution patterns in Africa: their relationship to variations in lithospheric and geological structure, and their rheological implications, Geophys. J. Int., **185**, (2011), 403-434.

Didana, Y.L., Thiel, S., Heinson, G.: Three dimensional conductivity model of the Tendaho High Enthalpy Geothermal Field, NE Ethiopia, Journal of Volcanology and Geothermal Research, **290**, (2015), 53-62.

Dugda, M.T., Nyblade, A.A., Julia, J., Langston, C.A., Ammon, C.J., and Simiyu, S.: Crustal structure in Ethiopia and Kenya from receiver function analysis: Implications for rift development in eastern Africa, J. Geophys. Res., **110** (2005), doi:10.1029/2004JB003065.

Ebinger, C.J., Deco, A.L., Drake, R. E., and Tesha, A.L.: Chronology of Volcanism and Rift Basin Propagation: Rungwe Volcanic Province, East Africa, J. Geophys. Res., **94**, (1989), 15785-15803.

Ebinger, C.J., Deino, A.L., Tesha, A.L., Becker, T., and Ring, U.: Tectonic Controls on Rift Basin Morphology: Evolution of the Northern Malawi (Nyasa) Rift, J. Geophys. Res., **98**, (1993), 17821-17836.

Ebinger, C.J., Rosendahl, B.R., and Reynolds, D.J.: Tectonic model of the Malawi rift, Africa, Tectonophysics, **141**, (1987), 215-235.

ELC-GDC: Reservoir Capacity Report. Under Provision of Consultancy Services for the Feasibility Study of Menengai Geothermal Power Project. November 2013. Unpublished.

ELC-GDC: Updated Reservoir Capacity Report. Under Consultancy Services for the Update of the Feasibility Study for 105 MW Menengai Geothermal Project. June 2015. Unpublished.

ELC-GSE: Conceptual Model Report. Prepared for GSE under Consultancy Services for Geothermal Surface Exploration in Tendaho Alalobeda, Ethiopia, February 2016. Unpublished.

ELC-TGDC: Kiejo-Mbaka Final Report. Prepared for TGDC under Surface Exploration and Training in Luhoi and Kiejo-Mbaka Geothermal Areas, project. October 2017. Unpublished.

ELC-TGDC: Luhoi Final Report. Prepared for TGDC under Surface Exploration and Training in Luhoi and Kiejo-Mbaka Geothermal Areas, project. February 2018. Unpublished.

GDC: Steam Status and Resource Assessment of Menengai Geothermal Project, Kenya. Internal Report (2018).

Giggenbach, W.F.: Geothermal solute equilibria. Derivation of Na-K-Mg-Ca geoindicators, Geochim. Cosmochim. Acta, **52**, (1988), 2749-2765.

Henry, W.J., Mechie, J., Maguire, P.K.H., Khan, M.A., Prodehl, C.,Keller, G.R., and Patel, J.; A seismic investigation of the Kenya Rift Valley, Geophys. J. Int., **100**, (1990), 107-130.

Kanda I., Fujimitsu, Y., and Nishijima, J.: Geological structures controlling the placement and geometry of heat sources within the Menengai geothermal field, Kenya as evidenced by gravity study, Geothermics, **79**, (2019), 67-81.

Keller, G.R., Prodehl, C., Mechie, J., Fuchs, K., Khan, M.A., Maguire, P.K.H., Mooney, W.D., Achauer, U., Davies, P.M., Meyer, R.P., Braile, L.W., Nyambok, I.O., and Thompson, G.A.: The East African rift system in the light of KRISP 90, Tectonophysics, 236, (1994), 465-483.

Lagat, J.: Geothermal surface exploration approach: case study of Menengai geothermal field, Kenya. Proceedings, Kenya Geothermal Conference (2011).

Last, R.J., Nyblade, A.A., and Langston, C.A.: Crustal structure of the East African Plateau from receiver functions and Rayleigh wave phase velocities, J. Geophys. Res., **102**, (1997), 24469-24483.

Leat, P.T.: Geological evolution of the trachytic caldera volcano Menengai, Kenya rift valley, Journal of the Geological Society, **141**, (1984) 1057-1069, doi: 10.1144/gsjgs.141.6.1057.

Maggi, A., Jackson, J.A., McKenzie, D., and Priestley K.: Earthquake focal depths, effective elastic thickness, and the strength of the continental lithosphere, Geology, **28**, (2000), 495-498.

Mibei, G., and Lagat, J.: Structural controls in Menengai geothermal field. Proceedings, Kenya Geothermal Conference 2011.

Mohr, P.A.: Nature of the crust beneath magmatically active continental rifts, Tectonophysics, **213**, (1992), 269-284.

Moeck, I.S.: Catalog of geothermal play types based on geologic controls, Renewable and Sustainable Energy Reviews, **37**, (2014), 867–882

Montegrossi, G., Pasqua, C., Battistelli, A., Mwawongo, G., and Ofwona, C.:3D Natural State Model of the Menengai Geothermal System, Kenya, Proceedings World Geothermal Congress 2015 Melbourne, Australia, 19-25 April 2015.

Mnjokava T., Kimani, A., Pasqua, C., Lelli, M., and Marini L.: Geochemistry of Kilambo-Kajala and Ilwalilo Hot Springs, Kiejo-Mbaka Geothermal Prospect, Tanzania Proceedings, 7th African Rift Geothermal Conference Kigali, Rwanda 31st October – 2nd November 2018

Mungania, J.: Overview of the geology of Menengai volcanic complex: Kenya Electricity Generating Company, Internal report (1999).

Omenda, .P.A.: The geothermal activity of the East African Rift, Presented at Short Course IV on Exploration for Geothermal Resources, organized by UNU-GTP, KenGen and GDC, at Lake Naivasha, Kenya, November 1-22, 2009.

Omenda, P.A: The geology and geothermal activity of the East African Rift, Short Course VII on Exploration for Geothermal Resources, organized by UNU-GTP, GDC and KenGen, in Naivasha, Kenya, 31st October - 23rd November 2013.

Omondi, C.: Borehole geology and hydrothermal mineralization of wells MW-01 and MW-02, Menengai geothermal field, Central Kenya Rift Valley, United Nation University, Geothermal Training Program, Iceland, Report, Number 30, (2011).

Pasqua, C.: Advances in the Exploration of Geothermal Resources of the East Africa Rift System (EARS), PH.D. Thesis, Doctoral Research of Science and Technology for Environment and Territory, Italy (2019).

Pasqua, C., Armadillo, E., Rizzello, D., Verdoya, M., Chiozzi, P., and Kebede, S.: Integrated analysis of geochemical and geophysical data from Alalobeda geothermal field Northern Afar region, Proceedings, 6th African Rift Geothermal Conference Addis Ababa, Ethiopia, 2nd - 4th November 2016,

Pasquale, V., Chiozzi, P. and Verdoya, M.: Tectonothermal processes and mechanical strength in a recent orogenic belt: Northern Apennines, J. Geophys. Res., **115**, (2010), doi:10.1029/2009JB006631.

Pellerin, L., Johnston, J.M., and Hohmann G.W.: A numerical evaluation of electromagnetic methods in geothermal exploration: Geophysics, **61**, (1996) 121-130, doi: 10.1190/1.1443931.

Prodehl, C., Jacobs, A.W.B., Thybo, E., Dindi, E., and Stangl, R.: Crustal structure on the northeastern flank of the Kenya rift, Tectonophysics, **236**, (1994), 271-290.

Prodehl, C. et al.,: The KRISP 94 lithospheric investigation of southern Kenya: the experiments and the main results, Tectonophysics, **278**, (1997) 121-147.

Rizzello, D., Armadillo, E., Pasqua C., Verdoya M., Kebede, S., Mengiste, A., and Giorgis G.H.: Three-dimensional geophysical modelling of the Alalobeda geothermal field, Proceedings, 6th African Rift Geothermal Conference Addis Ababa, Ethiopia, 2nd – 4th November 2016.

Rizzello, D., Armadillo, E., Pasqua, C., Pisani, P., Mnjokava, T., Mwano, J., Makoye, D., and Tumbu, L.: Three-dimensional geophysical modelling of Kiejo-Mbaka geothermal field, Tanzania, Proceedings, 7th African Rift Geothermal Conference Kigali, Rwanda 31st October - 2nd November 2018

Stamps, D.S., Calais, E., Saria, E., Hartnady, C., Nocquet, J.-M., Ebinger, C.J., and Fernandes, R.M.: A kinematic model for the East African Rift, Geophys. Res. Lett., **35**, (2008), doi:10.1029/2007GL032781.

Simiyu, S.M.: Application of micro-seismic method to geothermal exploration from the Kenya Rift: U. N. Short Course for Exploration for Geothermal Resources (2009).

Simiyu, S.M., and Keller, G.R.: An integrated geophysical analysis of the upper crust of the southern Kenya rift, Geophys. J. Int., **147**, (2001) 543-561.

Stimac, J., Armadillo E., Kebede S, Zemedkun M., Kebede Y., Teclu A,. Rizzello D., and Mandeno, P.E.: Integration and Modeling of Geoscience Data from the Tendaho Geothermal Area, Afar Rift, Ethiopia, Proceedings 5th African Rift geothermal Conference Arusha, (2014) Tanzania.

Tessema, A., and Antoine, L.A.G.: Processing and interpretation of the gravity field of the East African Rift: implication for crustal extension, Tectonophysics, **394**, (2004), 87– 110

Usshe, G., Harvey, C., Johnstone, R., and Anderson, E.: Understanding the resistivities observed in geothermal systems, Proceedings World Geothermal Congress 2000 Kyushu - Tohoku, Japan, May 28 - June 10, 2000.

Von Herzen R.P., and Vacquier, V.: Terrestrial heat flow in Lake Malawi, Africa, J. Geophys. Res., **72**, (1967), 4221-4226.

Waichel B.L., de Lima E.F., Sommer C.A., Lubachesky, R.: Peperite formed by lava flows over sediments: An example from the central Paraná Continental Flood Basalts, Brazil, Journal of Volcanology and Geothermal Research, **159**, (2007), 343-354.

Wamalwa, A.M., Mickus, K.L., and Serpa, L.F.: Geophysical characterization of the Menengai volcano, Central Kenya Rift from the analysis of magnetotelluric and gravity data, Geophysics, **78**, (2013), B187–B199.